Chapter 3

Interferometry for Online/In-Process Surface Inspection

Feng Gao

Additional information is available at the end of the chapter

http://dx.doi.org/10.5772/66530

Abstract

Interferometers are normally operated in environment-controlled optical laboratories because vibrations will induce errors in measurement results. In order to extend the application of interferometry to shop floor inspection, two methods are adapted: one method is to introduce a reference interferometer and vibration compensation system to the main interferometer, to compensate for the environmental disturbance; and the other method is to realize the data sample in just one image shot. Each method has its own applications. With the advances of these technologies, the use of interferometry as a highly accurate and fast measurement method will become more common in shop floor measurements and inspections.

Keywords: online/in-process measurement, surface measurement, environmental disturbance, vibration compensation, reference interferometer, common path

1. Introduction

The applications of optical interferometry are very extensive. It can be used to measure displacement, vibration, angle, distance, pressure, refractive index and temperatures, to just name a few. As a high accuracy and high sensitivity measurement method, interferometers are normally operated in optical laboratories in which operational environments are well controlled. Any variations such as temperature, air flow, air pressure and vibrations in the environment will induce errors to the measurement results and even make a measurement impossible to conduct. In this chapter, we will focus on discussions of the research conducted

in our research centre on the applications of optical interferometry at a shop floor environment, which is normally subjected to environmental disturbances and vibrations. These researches mainly focus on surface measurement and inspection, and this is the main focus of the research centre. The methods discussed here may also be applied to other application areas depending on the optical set-up of the interferometer system and the measurement objects.

The manufacture of highly added value components in developed economies is rapidly shifted to the design and production of micro-/nano-structured and free-form surfaces. The application of the use of micro-/nano-scale and ultra-precision structured surfaces is broad and covers the optics, silicon wafer, hard disks, MEMS/NEMS, micro-fluidics and micro-moulding industries. All these industries critically rely on ultra-precision surfaces. However, there is an essential factor to limit of the manufacture of these kinds of surfaces, that is to say the ability to measure the product quickly and easily within the manufacturing environment. According to the report, currently the quality of fabrication of these kinds of products depends mainly on the experience of process engineers backed up by an expensive trial-and-error approach. Subsequently, the scrap rates of these manufactured items are 50–70% high [1].

Optical interferometry has been extensively studied for surface measurement due to the advantages of non-contact measurement and high measurement accuracy. Nevertheless, conventional optical interferometry techniques are exceptionally sensitive to environmental noises such as air turbulence, temperature drift and mechanical vibration. Such noises can cause errors during surface measurement and produce void measurement results. There are a number of methods to reduce the influence of these noises. While controlling the measurement environment by using a vibration isolation stage and retaining a stable temperature is an effective way to reduce noise for laboratory and offline applications, it may not be practical in manufacturing conditions, for instance, when a measurement part is too large to be mechanically insulated.

In order to extend the application of interferometry to shop floor inspection, two methods can be adapted. One method is by introducing a reference interferometer and vibration compensation system to the main interferometer to compensate the environmental disturbance [2–4]. Complete common-path interferometers such as the scatterplate interferometer are insensitive to noises as well [5–7]. These noise reduction approaches are generally used for laser-based phase-shifting interferometry, for which the applications are limited to measurement of relatively smooth surfaces due to the well-known 2π phase ambiguity problem of monochromatic interferometry. The other method is to realize the data sampling in just one image shot [8–10]. This kind of so-called one shot interferometer is immune to the environmental noise and vibrations.

We will discuss the above two kinds of interferometry through two case studies: the common-path wavelength scanning interferometer and the single-shot line-scan dispersive interferometer.

http://dx.doi.org/10.5772/66530

2. Common-path wavelength scanning interferometer

2.1. Measurement principle

White light vertical scanning interferometry (WLSI) is able to overcome the 2π phase ambiguity problem and extend its application to rough surfaces and structured surfaces with large step heights [11–13]. It measures the optical path difference (OPD) by determining the peak position from the interferograms. It can be used to measure optically smooth surfaces as well as the optically rough surfaces. (The definition of an optically smooth surface is the surface height variation within the resolution cell of the imaging system is not exceed one-eighth of the wavelength of the light used. For optically rough surface which is defined as the height variations within the resolution cell of the imaging system is exceed one-fourth of the wavelength of the light used [13]). However, the need to perform a mechanical scanning of the heavy probe head or the specimen stage limits the measurement speed. In addition, the data acquisition procedure and processing are more complicated than monochromatic interferometry.

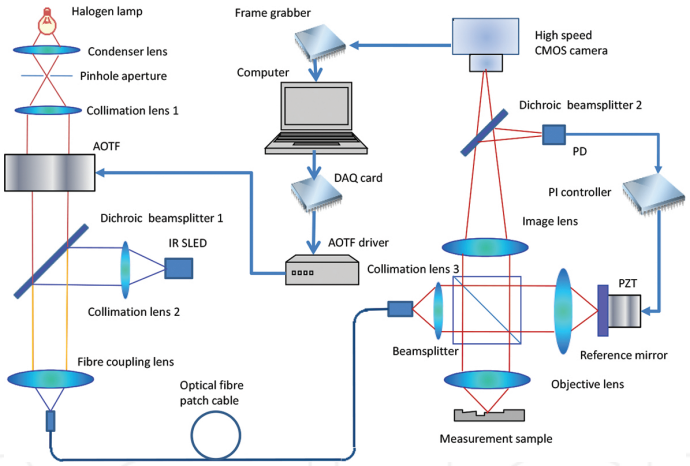

Figure 1. Schematic diagram of the proposed surface measurement system. AOTF–acousto-optic tuneable filter; PD–photo diode; IR SLED–inferred superluminescent light-emitting diode; DAQ–data acquisition card.

Wavelength scanning interferometry (WSI) has been reported by many researchers worldwide in areal surface measurement by using a two-dimensional CCD detector [4, 14–16]. Compared with WLSI, surface topography measurements are based on the phase shifts due to wavelength variations, thus avoiding any mechanical scanning process. Absolute optical path difference can be measured without any 2π phase ambiguity. WSI has advanced itself to dispersive white light interferometry [17, 18], measuring full field of surface instead of a single point of the surface by means of spectrometry.

We have proposed an environmentally robust fast surface measurement system by means of wavelength scanning interferometry and active servo control techniques. The basic configu-

ration of the proposed surface measurement system is illustrated in **Figure 1**. The measurement system is composed of two Linnik interferometers that share a common optical path. The measurement interferometer is illuminated by a white light source through an acousto-optic tuneable filter (AOTF) to filter the light from the white light source to the main interferometer. This is to select a specific wavelength for the interferometer, thus producing an interferogram at the CCD sourced only by that specific wavelength. The selected light wavelength is determined by:

$$\lambda = \Delta n \alpha \frac{v_a}{f_a} \tag{1}$$

where Δn is the birefringence of the crystal used as the diffraction material, α is a complex parameter subject to the design of the AOTF, and v_a and f_a are the velocity and frequency of the driving acoustic wave, respectively. The wavelength of the light which is selected by the AOFT can therefore be varied just by changing the driving frequency f_a. Consequently, different wavelengths of light will pass through the AOTF in sequence so a series of interferograms of different wavelengths will be detected by the CCD camera. The absolute optical path difference can be calculated in real time through analyzing interferograms captured by the CCD camera. The reference interferometer, which is illuminated by an inferred superluminescent light-emitting diode (SLED), is used to observe and compensate for the environmental noise, for example, mechanical vibration, temperature drift and air turbulence. Because the two interferometers undergo similar environmental noise, the measurement interferometer will be capable of measuring surface information once the reference interferometer is 'locked' into the compensation mode.

The light beams from the AOTF and the IR SLED are combined by a dichroic mirror that is highly reflective in the inferred wavelength and transmissive in the visible light wavelength range. After passing through the dichroic mirror, the light beam is coupled into an optical fibre patch cable. By separating the light source and AOTF from the interferometers, not only the size and weight of the interferometers have been greatly reduced, but also the thermal influence from the light source has also been eliminated.

It is well known that surface measurement in the workshop/manufacturing environment has been challenging to achieve using interferometric techniques since they are very sensitive to environmental vibrations, in particular, axial (vertical) vibration [5]. In addition, measurement noise can be induced by air turbulence and temperature drift as well. In this experimental study, the reference interferometer is illuminated by a SLED, which made by EXOLES (EXS2100068–01, 850 nm centre wavelength with 50 nm bandwidth) together with a servo feedback electronic unit to compensate the environmental noise effectively. Output light from the SLED is combined with the measurement light and travels virtually the same optical path as the measurement interferometer. The interference signal of the reference interferometer is picked up by a photodiode after being filtered off by dichroic beamsplitter 2 (Thorlabs, DMSP805 short pass dichroic mirror with 805 nm cut-off wavelength). As a result of a shared optical path, it is intended that if the noise happening in the reference interferometer is

http://dx.doi.org/10.5772/66530

monitored and compensated for; the measurement interferometer will not suffer any noise disturbance during measurement. The reference interferometer will be locked at about quadrature to maximize sensitivity to environmental instabilities through a piezoelectric transducer (PZT). The resolution of modern PZT can be up to 0.05 nm with a frequency response of 35 kHz (e.g. P-249.10, PI Company); the noise compensation can be quick and accurate provided the load is light. This technique has been tested effectively and proved in our previous research [6, 7].

2.2. Phase calculation principle

Intensities detected by pixel (x, y) of the CCD camera that correspond to one point on the test surface can be expressed by

$$I(x,y;k) = a(x,y;k) + b(x,y;k)\cos(2\pi kh(x,y)) \tag{2}$$

where $a(x, y; k)$ and $b(x, y; k)$ are the background intensity and fringe visibility, respectively, k is the wavenumber which is the reciprocal of wavelength, $h(x, y)$ and is the absolute optical path difference of the interferometer.

The phase of the interference signal $\varphi(x, y; k)$ is given by

$$\phi(x,y;k) = 2\pi kh(x,y). \tag{3}$$

The phase shift of the interference signal owing to the wavenumber shift is given by

$$\Delta\phi(x,y;\Delta k) = 2\pi\Delta kh(x,y). \tag{4}$$

The phase change of the interference signal is proportional to the wavenumber k change. Then, the optical path $h(x, y)$ difference is given by

$$h(x,y) = \frac{\Delta\phi(x,y,\Delta k)}{2\pi\Delta k}. \tag{5}$$

The change of k can be calibrated by using an optical spectral analyzer, and the key issue here is how to determine the phase change. There are many phase calculation algorithms that may be used in spectral scanning interferometry. These algorithms include phase demodulation by a lock in amplifier [19], and phase calculation by a seven-point method used in classical phase-shifting interferometry [20], extremum position counting [17] and Fourier transform-based techniques [21]. In this paper, we use phase calculation by Fourier transform because it is fast, accurate and insensitive to intensity noise.

In Eq. (2), as mentioned, *a(x, y; k)* and *b(x, y; k)* are slowly variable with respect to due to the response of *k* the CCD camera and the spectrum intensity of the light source. Practically, the optical path difference of the interferometer is adjusted to be large enough with the intention that the frequency of the cosine term is higher than the variation frequency of terms *a(x, y; k)* and *b(x, y; k)* so that they can be easily separated from each other. Eq. (2) can be rewritten as

$$I(x,y;k) = a(x,y;k) + \frac{1}{2}b(x,y;k)\exp[2\pi ikh(x,y)] + \frac{1}{2}b(x,y;k)\exp[-2\pi ikh(x,y)]. \tag{6}$$

The Fourier transform of Eq. (6) with respect to k can then be written as

$$\hat{I}(x,y;\xi) = A(x,y;\xi) + B(x,y;\xi - h(x,y)) + B(x,y;\xi + h(xy)) \tag{7}$$

where the uppercase letters denote the Fourier spectra of the signal expressed by the corresponding lower-case letters. If $h(x, y)$ is selected to be higher than the variation of $a(x, y, k)$ and $b(x, y, k)$, the three spectra can be separated from one another. To retrieve the phase distribution of the fringe, the term B(x, y; ξ−h(x, y)) is selected, and therefore, the background intensities $a(x, y, k)$ are filtered out. The inverse Fourier transform of B(x, y; ξ− h(x, y)) is

$$IFFT(B(x,y;\xi - h(x,y))) = \frac{1}{2}b(x,y;k)\exp[ikh(x,y)]. \tag{8}$$

Taking the natural logarithm of this signal yields,

$$\log\left\{\frac{1}{2}b(x,y;k)\exp[2\pi ikh(x,y)]\right\} = \log\left[\frac{1}{2}b(x,y;k)\right] + i\phi(x,y;k) \tag{9}$$

from which the imaginary part of Eq. (9) is exactly the phase distribution to be measured. Following the above processes, the phase distribution of each CCD pixel, as well as the height map of the surface to be measured, can be acquired. Because the main processes here are fast Fourier transform (FFT) and inverse fast Fourier transform (IFFT), the data processing is very fast.

2.3. Experimental results

The method described in the previous section was used to measure standard height specimens and different types of structured surfaces, for which two examples are presented here. In these experimental studies, the radio frequency applied to the AOTF (Model LSGDN-1, SIPAT Co.) was scanned from 80 to 110 MHz in steps of 10 kHz, equivalent to a wavelength interval of 0.48 nm. This range of radio frequencies provides a range of scanning wavelengths from 680.8 to 529.4 nm. Throughout the wavelength scanning process, 300 interferograms were captured

http://dx.doi.org/10.5772/66530

by a high-speed CCD camera (Model OK-AM1131, JoinHope Image Tech. Ltd.) at a frame rate of 100 frames/s. **Figure 2** shows the intensity distribution recorded by one of the CCD pixels (100, 100), and **Figure 2** shows the corresponding retrieved phase of this intensity distribution. It can be seen from **Figure 2** that this result suffers from discontinuities, where the values are in the range from $-\pi$ to π. These discontinuities have been amended by adding 2π at the discontinuous points to achieve a continuous phase distribution as shown in **Figure 2**. By using the continuous phase distribution, the sample step height of this pixel can be computed.

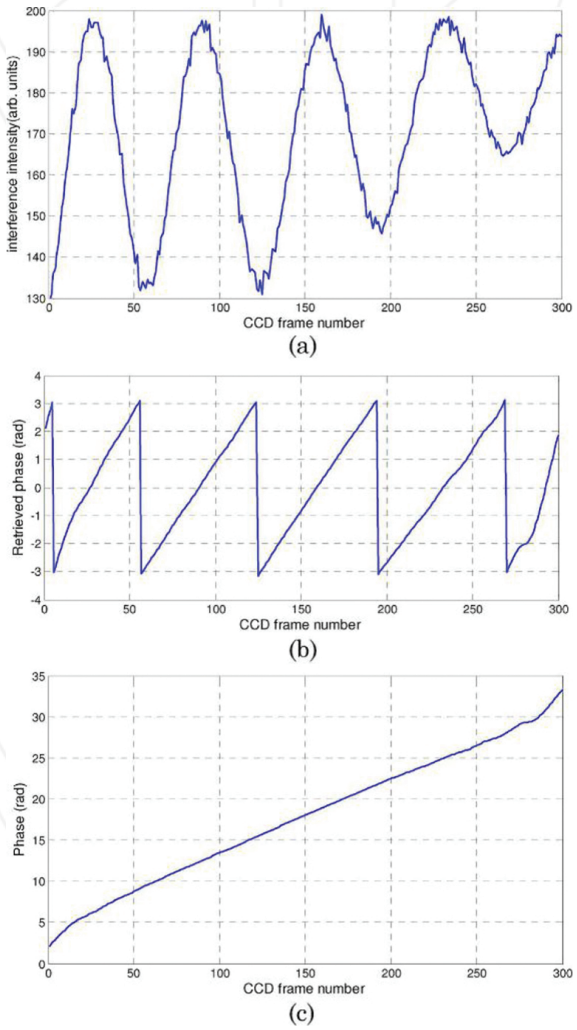

Figure 2. (a) Intensity distribution for 300 interferograms captured by a CCD pixel (100, 100), (b) retrieved phase discontinuous distribution, (c) phase continuity distribution.

A standard step height specimen with a calibrated step of 2.970 μm, provided by the National Physical Laboratory (NPL), UK, was used as a measurement sample. This specimen has been processed according to the above proposed measurement procedure and an areal surface view obtained as shown in **Figure 3**. The measured average step height is 2.971 μm with a measurement error of 1 nm.

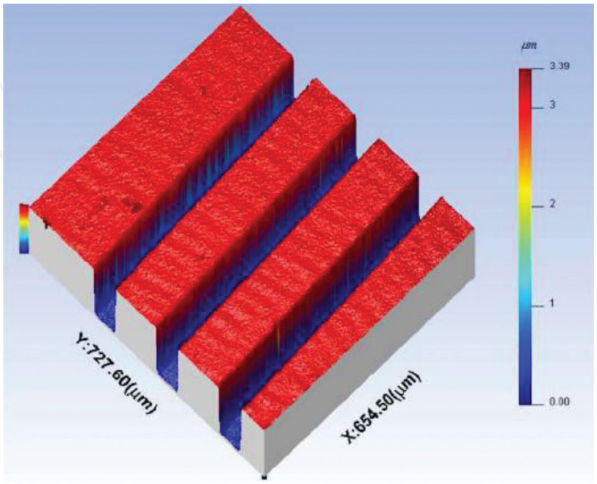

Figure 3. Measurement results of a 2.970 μm standard step.

The second measurement example is to investigate the effectiveness of the instrument's vibration compensation as follows:

1. A semiconductor daughterboard sample was measured without inducing mechanical disturbance. The measured surface step height is 4.756 μm (**Figure 4**);
2. A 40 Hz and 400 nm peak-to-peak sinusoidal mechanical disturbance using a PZT was applied to the reference mirror. During the disturbance, the measured surface step height is 11.711 μm (**Figure 5**). The surface roughness signal is completely distorted;
3. When the vibration compensation system is switched on, a decrease in the disturbance of the fringe pattern is clearly observed. A measurement of the sample is carried out with the vibration compensation system on. The data were retrieved as the original measurement and illustrate that the compensation vibration can be used to overcome environmental disturbance. The measured step height is 4.743 μm (**Figure 6**).

The difference between the two measured step height values is 13.5 nm. The measurement results are shown in **Figures 4–6**, respectively. The observed disturbance attenuation between parts (2) and (3) of the experiment was 12.2 dB, according to the reference interferometer signal output, which is in good agreement with the measured standard sample error.

http://dx.doi.org/10.5772/66530

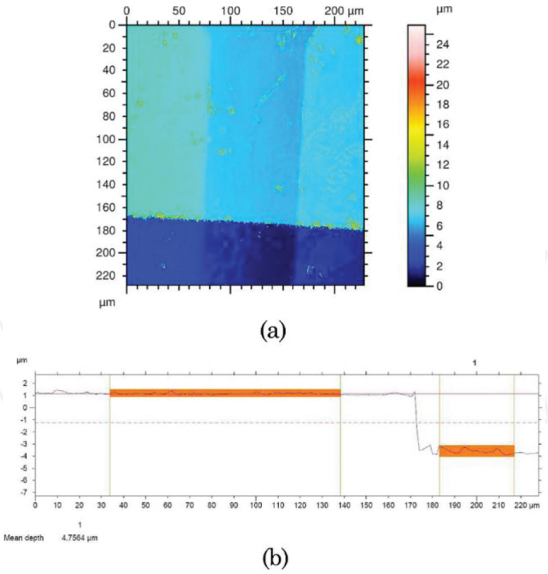

Figure 4. Measurement results of a semiconductor daughterboard sample without an induced mechanical disturbance: (a) measured surface and (b) cross-sectional profile.

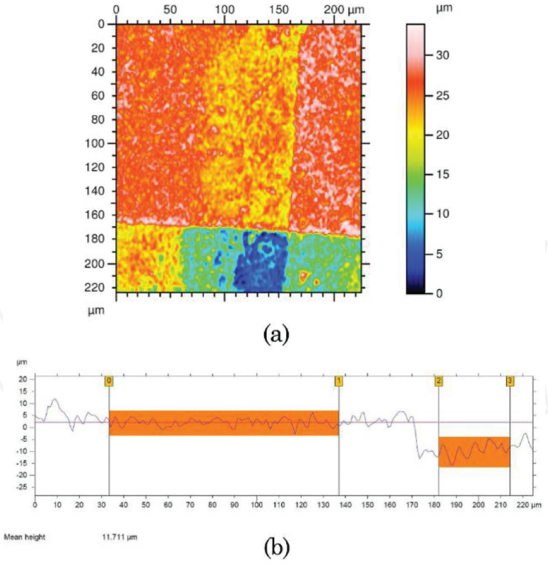

Figure 5. Measurement results of a semiconductor daughterboard sample with a sinusoidal mechanical disturbance of 40 Hz: (a) measured surface and (b) cross-sectional profile.

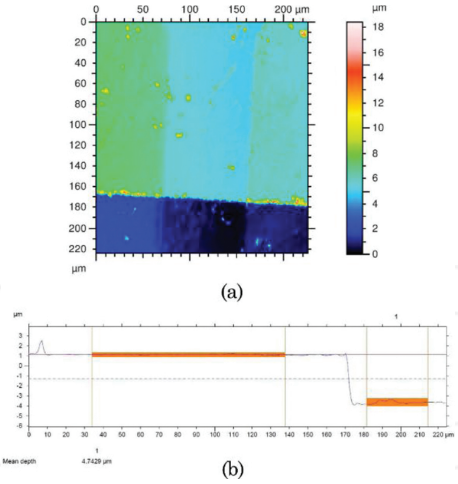

Figure 6. Measurement results of a semiconductor daughterboard sample with vibration compensation: (a) measured surface and (b) cross-sectional profile.

From the above case study, we can conclude that by using a common-path reference interferometer together with an active environmental noise compensation system, a wavelength scanning interferometer can be used for shop floor surface measurement.

Roll-to-roll (R2R) processing is a fast and economic processing method for manufacturers that produce high-volume products using large area foils such as packaging products, photovoltaic films and emerging market sectors such as flexible electronics. However, there is an increased risk of defects forming as the number of interfaces increases in the multi-layer films, and the size and nature of those defects change as the layer thicknesses shrink to the nanoscale [22, 23]. Because of the nature of these practices, the inspection methods have to be in non-contact with the film surfaces. Effective surface inspection is the key for further processes such as applying local repair techniques to eliminate the defects from the film surface.

The above system has been implemented into a R2R system for demonstration of online surface inspection [24]. Nevertheless, a measurement can only be achieved if the measured sample is at a standstill. However, the tested sample surface is in constant movement during inspection, due to the nature of R2R processing. In order to achieve dynamic inspection, all the measurement information must be sampled in just one sample, and the sampling rate should be greater than a few hundred Hz to reduce the effect of mechanical vibration. In this case, a dynamic interferometer [8–10] is the solution. However, these approaches have one drawback for the application of online surface measurement: the 2µ phase ambiguity for phase-shift interferometer, which restricts the vertical measurement range to a few hundred nanometres. It is short of the demands of most surface measurements and inspections. We have introduced a single-shot line-scan dispersive interferometer [25] which is able to perform dynamic surface inspection and has a vertical measurement range over a few hundred micrometers.

http://dx.doi.org/10.5772/66530

3. Single-shot line-scan dispersive interferometer

3.1. Experimental set-up

The basic configuration of the proposed line-scan dispersive interferometer (LSDI) is shown in **Figure 7**. A halogen bulb with broadband spectrum is used to generate the white light illumination for the system. This low-coherence white light is coupled into a multi-mode optical fibre patch cable with a numerical aperture of 0.39. The tested surface is observed through a 4 × Michelson interferometric objective. The interfered beam is focused using a tube lens with a focal length of 250 mm and split into two parts by a pellicle beamsplitter coated with a 45:55 (reflectance: transmission) split ratio. The reflectance part is received by camera 1 which provides real-time imaging of the observed surface. The other part is brought to a spectrometer to generate spectral interferograms for surface measurement. More specifically, this transmission beam first passes through a slit to block the light redundant for measurement, after that a narrow line of light which represents an interference signal of a surface profile is selected and diffracted by the grating and finally received on camera 2. The direction of the slit is set to be parallel to the columns of camera pixels, so that the dispersion axis is along the rows.

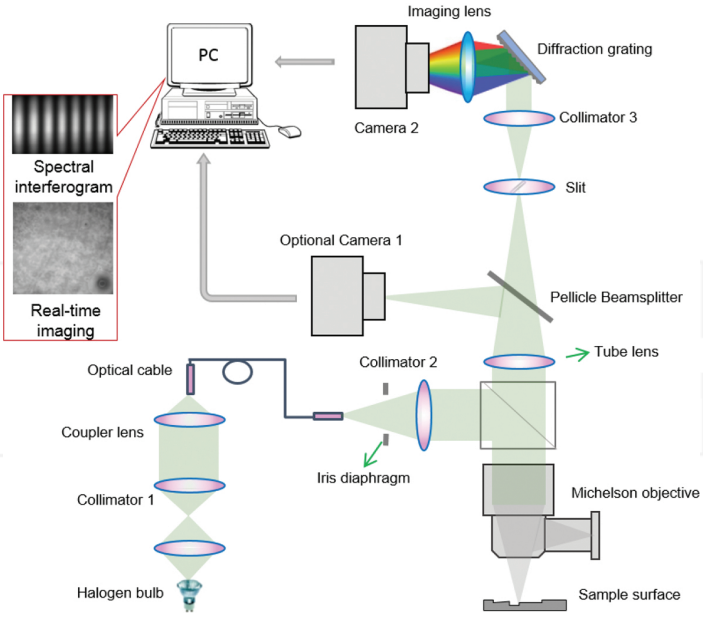

Figure 7. Schematic diagram of the optical set-up.

3.2. Interferograms analysis

Many algorithms have been developed to extract the phase from the spectral interferograms, including the techniques based on fast Fourier transform (FFT) [26], convolution [27] and Hilbert transform [28]. We developed a FFT-based algorithm for the proposed system because it is effective, accurate and insensitive to intensity noise [5]. The developed algorithm for interpreting the captured interferograms contains five sections, as shown in the flowchart which follows (**Figure 8**).

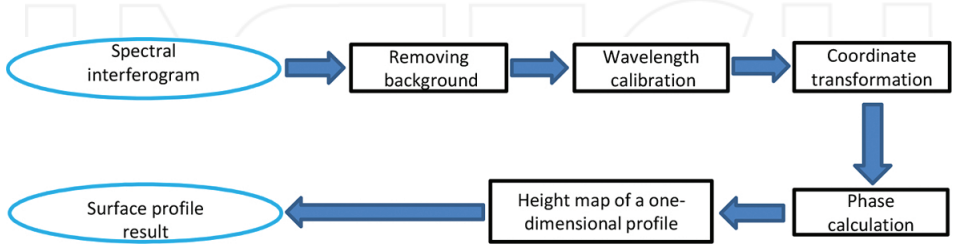

Figure 8. Flowchart of the FFT-based algorithm.

3.2.1. Removing background

The recorded interferogram contains a background intensity variation which is generated by the spectral distribution of the light source and the spectral response of the CCD camera. By blocking the measurement arm of the interferometer, a reference frame without interference effect can be captured and afterwards removed from each spectral interferogram.

3.2.2. Wavelength calibration

The output of the spectrometer is spectrally decomposed along the rows (or columns) of CCD pixels. For example, if a diffraction grating has space d, when a plane wave is incident with an angle θ_i, and the diffraction angle is θ_m to the order m, then for a beam with wavelength λ, the following equation should be satisfied

$$m\lambda = d(\sin\theta_i + \sin\theta_m). \tag{10}$$

Grating Eq. (10) shows that the relationship between the dispersed wavelength and pixel number is not linear. Therefore, the exact relationship between the pixel number and the specific wavelength needs to be calibrated. A white light laser source (WhiteLase™ micro) in conjunction with the acoustic-optical tuneable filter (AOTF) is used for the calibration. The specific wavelength selected by the AOTF is determined by Eq. (11)

$$\lambda = \Delta n \alpha v_a * (f_a)^{-1}. \tag{11}$$

http://dx.doi.org/10.5772/66530

A second-order polynomial is used to represent the relationship between pixel number and wavelength, as shown in Eq. (12)

$$\lambda_p = Ap^2 + Bp + C \tag{12}$$

where λ_P is the wavelength of pixel p, C is the wavelength of pixel 0, B is the first-order coefficient (nm/pixel), and A is the second-order coefficient (nm/pixel^2). More than 30 groups of experimental data (spectral lines) have been recorded to calculate the values for A, B and C through the least squares equation. The calibration result is depicted in **Figure 9**.

3.2.3. Coordinate transformation

The original signal obtained is a curve of irradiance with respect to wavelength λ (or pixel number). However, the phase variation extracted from the channelled spectrum is linearly related to the wavenumber $\sigma(\sigma = 1/\lambda)$, which makes the coordinate transformation necessary. The original sinusoidal signals are resampled in equal intervals through spline interpolation and finally reconstructed to a wavenumber-related curve.

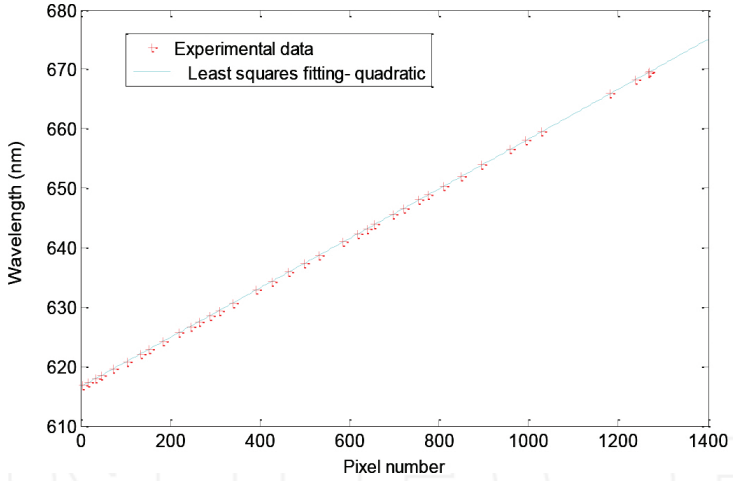

Figure 9. Wavelength calibration of the CCD camera.

3.2.4. Phase calculation

As mentioned above, we use FFT to extract the phase from the spectral interferogram. The spectral intensity $I(\mathrm{h}, \sigma)$ recorded at the output of the spectrometer can be expressed as

$$I(x,y;\sigma) = a(x,y;\sigma) + b(x,y;\sigma)\cos[\varphi(x,y;\sigma)] \tag{13}$$

where $I(x, y; \sigma)$ is the normalized intensity with background intensity variation removed, (x, y) denotes the spatial coordinates of the interferogram, $a(x, y; \sigma)$ and $b(x, y; \sigma)$ represent the background intensity and fringe visibility, respectively, and the phase $\varphi(x, y; \sigma)$ is defined by formula

$$\varphi(x,y;\sigma) = 4\pi\lambda^{-1} \times h(x,y) + \varphi_0 = 4\pi\sigma h(x,y) + \varphi_0 \tag{14}$$

where $h(x, y)$ represents the surface elevation, and ϕ_0 is the initial phase. Eq. (13) can be written in another form as Eq. (15)

$$I(x,y;\sigma) = a(x,y;\sigma) + c(x,y;\sigma) + c^*(x,y;\sigma) \tag{15}$$

with

$$c(x,y;\sigma) = \frac{1}{2} b(x,y;\sigma) \exp[i\ \varphi(x,y;\sigma)] \tag{16}$$

where * denotes a complex conjugate. Fourier transform on the original spatial signals can be expressed in frequency domain as Eq. (17)

$$\tilde{I}(x,y;f) = A(x,y;f) + C(x,y;f) + C^*(x,y;f) \tag{17}$$

where the capital letters denote the Fourier spectra, and f is the spatial frequency. The unwanted background variation is removed by setting a filtration window, and then, the desired term $C(x, y, f)$ is selected to compute the inverse fast Fourier transform (IFFT). Taking the natural logarithm of the IFFT $[C(x, y; f)]$, the phase $\varphi(x, y; \sigma)$ of each point is extracted as the imaginary part of the Eq. (18)

$$log\left\{\frac{1}{2} b(x,y;\sigma) \exp[i\ \varphi(x,y;\sigma)]\right\} = log\left[\frac{1}{2} b(x,y;\sigma)\right] + i\ \varphi(x,y;\sigma). \tag{18}$$

Finally, the phase unwrapping process, illustrated in detail by Takeda et al. in 1982 [26], is performed to the discontinuities phase distribution.

3.2.5. Height map of a one-dimensional profile

The vertical axis of the spectral interferogram represents one dimension of lateral resolution, which means each row signal contains the height information of one point. By using the phase slope S obtained from the phase calculation process, the height value can be acquired

http://dx.doi.org/10.5772/66530

using Eq. (19). After analysis of a series of row signals, the height map of a surface profile can be obtained.

$$h = \frac{S}{4\pi} = \Delta\varphi^{*}[4\pi(\sigma_m - \sigma_n)]^{-1} \tag{19}$$

where σ_m and σ_n> are the wavenumbers corresponding to the phase difference $\Delta\phi$.

3.3. Results and discussion

Two surface samples were measured to evaluate the performance of the prototype. First, to verify a good accuracy and measurement repeatability of the system, a standard sample from the National Physical Laboratory (NPL) with a step height of 100.0 nm was measured 24 times as shown in **Figure 10**. The measured average heights were recorded. It was found that the mean value of these 24 values is 96.6 nm, and the standard deviation was then calculated as 8.2 nm using Eq. (20).

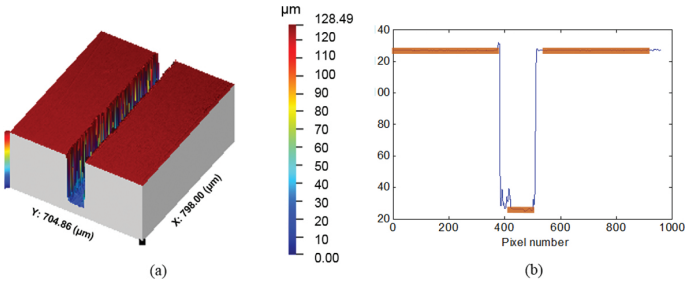

Figure 10. Measurement result of a micro-fluid chip with 100 μm step height: (a) 3D surface map, (b) cross-sectional profile.

$$\sigma = \left(\sum_{i=1}^{N} (H_i - \bar{H})^2 * (N-1)^{-1} \right)^{\frac{1}{2}}. \tag{20}$$

The second sample we measured was a multi-layer polyethylene naphthalate (PEN) film manufactured by the Centre for Process Innovation (CPI). This thin film is composed of three layers, namely a PEN substrate layer (125 μm), a planarization layer (3–4 μm) for planarising the pit and spike features on the PEN substrate, and an atomic layer deposition (ALD) barrier (40 nm) for prevention of moisture and oxygen ingress. The results acquired by a Taylor-Hobson Coherence Correlation Interferometry (CCI) instrument (Talysurf CCI 3000) and LSDI are shown in **Figure 11** and **Figure 12**. The 3D surface map shown in **Figure 11** is generated by 1400 profiles, which represents a scanning length of 2.31 mm. The surface topography

results shown in **Figure 11** have different forms because different surface tensions are generated when fixing this film sample in these two separate measurements. Both 3D and 2D surface topography results demonstrate that LSDI is capable of detecting most of defects as the CCI does and the relative positions between each defect are well matched.

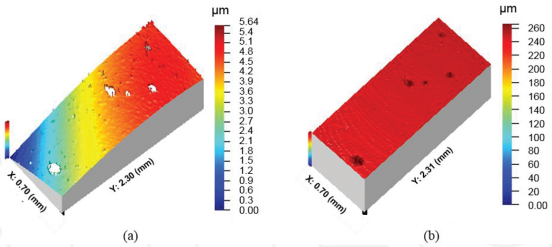

Figure 11. Defects detection on the Al_2O_3 ALD barrier film surface: (a) 3D surface map result using CCI and (b) result using LSDI.

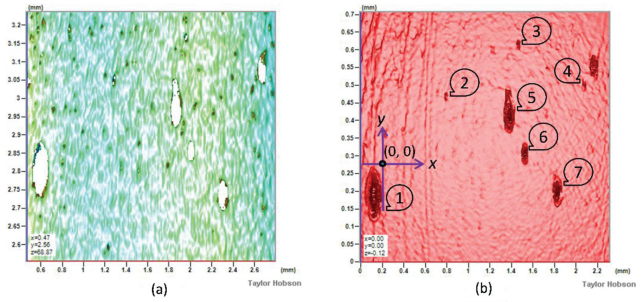

Figure 12. 2D view of defects on the Al_2O_3 ALD barrier film surface: (a) CCI result and (b) LSDI result.

	Size width × length (mm)		**Position (x, y) (mm)**	
	WLCSI	**CCI**	**WLCSI**	**CCI**
Defect 1	0.17 × 0.15	0.16 × 0.15	Reference point (0, 0)	
Defect 2	0.03 × 0.04	0.03 × 0.04	(0.61, 0.21)	(0.62, 0.19)
Defect 3	0.05 × 0.03	0.05 × 0.03	(1.29, 0.36)	(1.30, 0.30)
Defect 4	0.05 × 0.03	0.04 × 0.03	(1.90, 0.24)	(1.92, 0.16)
Defect 5	0.12 × 0.14	0.12 × 0.14	(1.24, 0.23)	(1.25, 0.18)
Defect 6	0.08 × 0.06	0.08 × 0.05	(1.36, 0.07)	(1.37, 0.00)
Defect 7	0.10 × 0.09	0.10 × 0.09	(1.68, −0.03)	(1.68, −0.10)

Table 1. Defects' specifications (size, location).

Analysis results of defects specifications for both CCI and LSDI are listed in detail in **Table 1**. The sizes and positions (x axis) of the defects correlate well between the CCI measurement of the sample and the measurement performed using LSDI. The slight difference of the relative positions along the y axis is due to different surface tensions as mentioned above, which does not affect the assessment of LSDI's performance.

The results above verified that LSDI performs well in defects detection. Only one shot for a surface profile makes it a fast and environmentally robust measurement system.

4. Conclusion

Two case studies for online surface measurement by means of interferometry have been discussed. The first case study presents a surface measurement technique with active control of environmental noise and disturbance. Nanometre accuracy surface measurement results have been obtained for micrometre step height samples. Disturbance has been reduced by 12.2 dB at 40 Hz vibration frequency. The second case study presents a line-scan dispersive interferometer with a good lateral resolution and nano-scale measurement repeatability. It has an extended axial measurement range by dispersing the output of the spectrometer along the camera pixels, without the 2π phase ambiguity. Free from any mechanical scanning and obtaining a surface profile in a single shot allows this set-up to minimize the effect of external perturbations and environmental noise.

Acknowledgements

The author gratefully acknowledges the UK's Engineering and Physical Sciences Research Council (EPSRC) funding of the EPSRC Centre for Innovative Manufacturing in Advanced Metrology (Grant Ref: EP/I033424/1), the funding with Grant Ref: EP/K018345/1 and the funding of the EPSRC HVMC Fellowship.

Author details

Feng Gao

Address all correspondence to: f.gao@hud.ac.uk

Centre for Precision Technologies, University of Huddersfield, UK

References

[1] L. Singleton, R. Leach, A. Lewis and Z. Cui, "Report on the analysis of the MEMSTAND survey on Standardisation of MicroSystems Technology," MEMSTAND Project IST-2001-37682 (2002), Proceedings of the International Seminar MEMSTAND - "Standardisation for Microsystems: the Way Forward"., 24–26 February 2003, Barcelona, Spain, 11–31.

[2] X. Jiang and D. Whitehouse, "Miniaturized optical measurement method for surface nanometrology," Annals of the CIRP,55, 1 (2006).

[3] X. Jiang, K. Wang and H. Martin, "Near common-path optical fiber interferometer for potential fast on-line microscale-nanoscale surface measurement," Optics Letters, 31, 3603–3605 (2006).

[4] X. Jiang, K. Wang, F. Gao and H. Muhamedsalih, "Fast surface measurement using wavelength scanning interferometry with compensation of environmental noise," Applied Optics, 49(15), 2903–2909 (2010). ISSN 1559–128X.

[5] M. North-Morris, J. Van Delden and J. Wyant, "Phase-shifting birefringent scatterplate interferometer," Applied Optics, 41(4), 668–677 (2002).

[6] J. Huang, T. Honda, N. Ohyama, and J. Tsuiiuchi, "Fringe scanning scatter plate interferometer using a polarized light," Optics Communications, 68, 235–238 (1988).

[7] D. Su and L. Shyu, "Phase-shifting scatter plate interferometer using a polarization technique," Journal of Modern Optics, 38, 951–959 (1991).

[8] C. Koliopoulos, "Simultaneous phase-shift interferometer," Proceedings of SPIE, 1531, 119–127 (1992).

[9] J. E. Millerd and N. J. Brock, "Methods and apparatus for splitting, imaging, and measuring wavefronts in interferometry," U.S. Patent 6,304,330 (2001).

[10] N. I. Toto-Arellano, G. RodrÍguez-Zurita, C. Meneses-Fabian, and J. F. Vazquez-Castillo, "Phase shifts in the Fourier spectra of phase gratings and phase grids: an application for one shot phase-shifting interferometry," Optics Express, 16, 19330–19341 (2008).

[11] G.KinoandS.Chim,"Miraucorrelationmicroscope,"AppliedOptics,29,3775–3783(1990).

[12] L. Deck and P. de Groot "High-speed noncontact profiler based on scanning white light interferometry," Applied Optics, 33, 7334–7338 (1994).

[13] T. Dresel, G. Hausler, and H. Venzke, "Three-dimensional sensing of rough surfaces by coherence radar," Applied Optics 31, 919–925 (1992).

[14] S. Kuwamura, and I. Yamaguchi, "Wavelength scanning profilometry for real-time surface shape measurement microscope," Applied Optics 36, 4473–4482 (1997).

[15] A. Yamamoto, C. Kuo, K. Sunouchi, S. Wada, I. Yamaguchi and H. Tashiro, "Surface shape measurement by wavelength scanning interferometry using an electronically tuned Ti: sapphire laser", Optical Review, 8, 59–63 (2001).

[16] A. Yamamoto and I. Yamaguchi, "Surface profilometry by wavelength scanning Fizeau interferometer", Optics Laser and Technology, 32, 261–266 (2000).

[17] J. Schwider and L. Zhou, "Dispersive interferometric profilometer, " Optics Letters, 19(13), 995–997 (1994).

[18] U. Schnell, R. Dandliker and S. Gray, "Dispersive white-light interferometry for absolute distance measurement with dielectric multilayer systems on the target", Optics Letters, 21(7), 528–530 (1996).

[19] X. Dai, and S. Katuo, "High-accuracy absolute distance measurement by means of wavelength scanning heterodyne interferometry," Measurement Science and Technology, 9, 1031–1035 (1998).

[20] P. Sandoz, G. Tribillon and H. Perrin, "High-resolution profilometry by using phase calculation algorithms for spectroscopic analysis of white-light interferograms," Journal of Modern Optics, 43(4), 701–708 (1996).

[21] M. Takeda and H. Yamamoto, "Fourier-transform speckle profilometry: three-dimensional shape measurements of diffuse objects with large height steps and/or spatially isolated surfaces," Applied Optics, 33(34), 7829–7837 (1994).

[22] B. Parida, S. Iniyan and R. Goic., "A review of solar photovolataic technologies," Renewable and sustainable Energy Reviews, 15, 1625–1636 (2011).

[23] F. C. Krebs, "Fabrication and processing of polymer solar cells: a review of printing and coating techniques," Solar Energy Materials & Solar Cells, 93, 394–412 (2009).

[24] F. Gao, et al. "A flexible PV barrier films defects detection system for in-situ R2R film processing". In: Special Interest Group Meeting: Structured Freeform Surfaces 2014 Programme, 19–20 Nov 2014, Padova, Italy (2014).

[25] D. Tang, F. Gao and X. Jiang, "On-line surface inspection using cylindrical lens-based spectral domain low-coherence interferometry" Applied Optics, 53(24), 5510–5516 (2014). ISSN 1559–128X.

[26] M. Takeda, H. Ina and S. Kobayashi, "Fourier-transform method of fringe-pattern analysis for computer-based topography and interferometry", Journal of the Optical Society of America, 72, 156–160, (1982).

[27] C. Sainz, J. Calatroni, and G. Tribillon, "Refractometry of liquid samples with spectrally resolved white light interferometry," Measurement Science and Technology, 1, 356–61 (1990).

[28] S. Debnath and M. Kothiyal, "Analysis of spectrally resolved white light interferometry by Hilbert transform method", SPIE Optics + Photonics. International Society for Optics and Photonics (2006), Proceedings of SPIE Volume 6292.

INTECH